AAC Journals.ASM.org

Alkaloids as Inhibitors of Malate Synthase from *Paracoccidioides* spp.: Receptor-Ligand Interaction-Based Virtual Screening and Molecular Docking Studies, Antifungal Activity, and the Adhesion Process

Fausto Guimaraes Costa,[b] Benedito Rodrigues da Silva Neto,[a] Ricardo Lemes Gonçalves,[b] Roosevelt Alves da Silva,[b] Cecília Maria Alves de Oliveira,[c] Lucília Kato,[c] Carla dos Santos Freitas,[c] Maria José Soares Mendes Giannini,[d] Julhiany de Fátima da Silva,[d] Célia Maria de Almeida Soares,[a] Maristela Pereira[a]

Laboratório de Biologia Molecular, Instituto de Ciências Biológicas, Universidade Federal de Goiás, Goiânia, Goiás, Brazil[a]; Núcleo Colaborativo de BioSistemas, Regional Jataí, Universidade Federal de Goiás, Jataí, Goiás, Brazil[b]; Laboratório de Produtos Naturais, Instituto de Química, Universidade Federal de Goiás, Goiânia, Goiás, Brazil[c]; Laboratório de Micologia Clínica, Universidade Estadual Júlio de Mesquita Melo, Araraquara, São Paulo, Brazil[d]

***Paracoccidioides* is the agent of paracoccidioidomycosis. Malate synthase plays a crucial role in the pathogenicity and virulence of various fungi, such as those that are human pathogens. Thus, an inhibitor of this enzyme may be used as a powerful antifungal without side effects in patients once these enzymes are absent in humans. Here, we searched for compounds with inhibitory capacity against the malate synthase of *Paracoccidioides* species (*Pb*MLS). The three-dimensional (3D) structure of *Pb*MLS was determined using the I-TASSER server. Compounds were selected from the ZINC database. Based on the mechanism underlying the interaction of the compounds with *Pb*MLS, it was possible to identify β-carboline moiety as a standard key structure. The compounds with β-carboline moiety that are available in our laboratories were investigated. A total of nine alkaloid compounds were selected. The primary mechanisms of interaction of the alkaloid compounds in the binding pocket of *Pb*MLS were identified and compared with the mechanism of interaction of acetyl coenzyme A (acetyl-CoA). We discovered that the amphipathic nature of the compounds, concomitant with the presence of β-carboline moiety, was crucial for their stability in the binding pocket of *Pb*MLS. In addition, the importance of a critical balance of the polar and nonpolar contacts of the compounds in this region was observed. Four β-carboline alkaloid compounds showed the ability to inhibit recombinant *Pb*MLS (*Pb*MLSr) activity, *Paracoccidioides* species growth, and adhesion of the fungus and *Pb*MLSr to the extracellular matrix components. The cytotoxicity of the alkaloids was also evaluated.**

Several plants, human-pathogenic fungi, and bacteria utilize the glyoxylate cycle during host infection (1). The unique enzymes of this cycle are isocitrate lyase and malate synthase. This pathway has not been observed in mammals; therefore, this cycle has been identified as a potential target for the discovery of new drugs. Novel active molecules should shorten the duration of chemotherapy, prevent the development of resistance, and eliminate latent disease.

In the human-pathogenic fungi from the genus *Paracoccidioides*, the malate synthase (*Pb*MLS) participates in the glyoxylate pathway, which enables the fungus to assimilate two-carbon compounds, and in the allantoin degradation pathway associated with purine metabolism, which allows the fungus to use nitrogen compounds (2). *Pb*MLS is localized in peroxisomes and on the cell surface and is secreted. In addition, *Pb*MLS plays a role as an adhesin, mediating the adhesion and internalization of the fungus to host cells (3). *Pb*MLS is regulated during the transition from mycelium to yeast (4) and in oxidative stress (5). However, an inhibitor to *Pb*MLS has not yet been investigated.

In recent years, virtual screening has become an accepted tool in drug discovery that has successfully been applied in a number of therapeutic programs, particularly at the lead discovery stage, during which high-throughput molecular docking can play an important role (6, 7). Receptor-ligand interaction-based virtual screening can dock each molecule of a library into the receptor binding site of a known or predicted three-dimensional (3D) structure to predict the highest affinity between a protein and its ligands (8). The molecules of the library are ranked according to their predicted binding affinity with the receptor. In addition to the time and cost savings associated with the discovery of ligands for a protein target, an additional benefit is the increased specificity of the predicted ligands, because receptor-ligand interaction-based virtual screening is directed against a known binding site or even against a particular receptor conformation (9).

The analysis of the chemical structure of the compounds from virtual screening revealed that the top compounds selected by the affinity and efficiency parameters had structural similarity to the β-carboline alkaloids, mainly due to its indole moiety. In addition, the literature survey showed that this class of alkaloids has a

Received 12 November 2014 **Returned for modification** 15 February 2015
Accepted 22 June 2015

Accepted manuscript posted online 29 June 2015

Citation Costa FG, Neto BRDS, Gonçalves RL, da Silva RA, de Oliveira CMA, Kato L, Freitas CDS, Giannini MJSM, da Silva JDF, Soares CMDA, Pereira M. 2015. Alkaloids as inhibitors of malate synthase from *Paracoccidioides* spp.: receptor-ligand interaction-based virtual screening and molecular docking studies, antifungal activity, and the adhesion process. Antimicrob Agents Chemother 59:5581–5594. doi:10.1128/AAC.04711-14.

Address correspondence to Maristela Pereira, maristelaufg@gmail.com.

F.G.C. and B.R.D.S.N. contributed equally to this work.

Supplemental material for this article may be found at http://dx.doi.org/10.1128/AAC.04711-14.

doi:10.1128/AAC.04711-14

range of biological activity (10), including antifungal activity against *Candida albicans* (11). Next, a series of β-carboline alkaloids isolated by our research group from *Rubiaceae* and *Apocynaceae* species were introduced in this study.

In this paper, we report candidate inhibitors of *Pb*MLS that were obtained through receptor-ligand interaction-based virtual screening and molecular docking studies and β-carboline alkaloids that inhibit *Pb*MLS, *Paracoccidioides* spp., and the adhesion process. The cytotoxicity of the alkaloids was also evaluated.

MATERIALS AND METHODS

Receptor preparations. Here, we propose a homology-based model of *Pb*MLS based on the 3D structures of *Escherichia coli* and *Bacillus anthracis* malate synthase A (PDB ID: 3CV1A) as the template (12), because the 3D structure of *Pb*MLS has not been resolved. This model was built using the I-TASSER server (13). The quality of the predicted structure was assessed using the NIH-Molecular Biology Institute (MBI) laboratory servers with Errat (14). The Ramachandran plot of *Pb*MLS was prepared on the RAMPAGE Web server (15), and the Verify3D server was used to evaluate the environments of the amino acids (16). The molecular dynamics (MD) simulations of this structure were performed with Gromacs (17–19) to reproduce the structural stability of this receptor in its native environment. The protocol used here to structure refinement is the same as that recently used to predict the structure of the glyoxylate cycle of *Paracoccidioides* spp. (*Pb*ICL) (20).

Ligand preparations. The structures of compounds were obtained from the ZINC database (21). A total of 89,415 compounds were selected for testing without any selection criteria and without any modification to the original files. The 3D structures of the alkaloid compounds were generated using the GlycoBioChem PRODRG2 server (22).

Molecular docking. Molecular docking tests were performed with AutoDock Vina (23) limited to a grid involving all pockets of the protein, which were defined using DoGSiteScorer, an active-site prediction and analysis server (24). The grid was defined using MGLTools to involve the pockets of *Pb*MLS. In this case, to increase the efficiency of the sampling, 1,000 independent simulations were performed in addition to those already performed using AutoDock Vina, with an exhaustiveness of 8. AutoDock Vina uses a conformation-independent function, *g*, given by

$$g = \frac{c_{\text{inter}}}{1 + wN_{\text{rot}}} \quad (1)$$

where N_{rot} is the number of active rotatable bonds between the heavy atoms in the ligand (torsions), and *w* is the associated weight. Because of the exhaustive sampling performed for each ligand, we nullified the effects of torsion considered in equation 1 and defined the term c_{inter} as the AutoDock Vina energy and the *g* values as the AutoDock Vina scores. The function c_{inter} is able to incorporate the main contributions to the binding free energy, which depends on the distance between the atoms. The interactions of type H-bonds, π or σ interactions (PI), and sigma interactions were not treated separately but were effectively merged into a dependent function of the distance between the atoms.

Ligand efficiency. Abad-Zapatero (25) proposed a simple function able to select compounds not only by affinity but also by efficiency criteria. Such function depends on the binding energy Δ*G* between the ligand and receptor and the total number (*n*) of atoms, which classifies the efficiency of ligands (EL) according to their size. Compounds with fewer atoms and higher affinity are considered more efficient. To this end, we replaced Δ*G* in equation 2 by the AutoDock Vina score to proceed with the selection of ligands with a lower binding energy, because the score is limited to a maximum preset. This ensures the selection of small ligands and stability in the binding pocket:

$$\text{EL} = \frac{\Delta G}{n} \quad (2)$$

Virtual screening. Using AutoDock Vina, a total of 89,415 compounds in the ZINC database were screened using its function score. Two types of classification criteria were established: (i) affinity, involving the selection of 10 compounds depending on the energy profile, and (ii) efficiency, involving the selection of the 10 compounds with the lowest EL (efficiency ligands; see equation 2) values and limited to a maximum score of −8.0 kcal/mol. In this stage, the selection of the 10 compounds also depended on the energy profile.

Based on the affinity criterion, we initially selected only the 100 ligands that exhibited the lowest scores, as determined by AutoDock Vina. For each ligand, 1,000 independent simulations were performed to construct histograms of the lowest energies achieved in each simulation, which helped the selection of ligands with stability but also those with more clearly defined states. The ligands with a number of occurrences of >50% in a given energy/conformation were considered successful. However, if this condition was not satisfied, the ligands were not ranked by their scores. For simulations involving alkaloids, a score histogram was also built for each compound.

A flowchart for the screening of compounds by affinity and efficiency is depicted in Fig. S1 in the supplemental material, which consists of three stages: (i) receptor prediction, (ii) compound selection, and (iii) features of the inhibitor alkaloids against *Pb*MLS. The solvent-accessible surface area (ASA) of each compound was calculated using the get_area function in PyMOL (PyMOL molecular graphics system; Schrödinger).

Experimental chemistry. Monoterpene β-carboline alkaloids 1 through 3 were isolated from *Psychotria prunifolia* (26). Alkaloids 4 and 5 were isolated from *Galianthe ramosa* (27), alkaloids 6 and 7 were isolated from *Rauvolfia bahiensis* (28), and alkaloids 8 and 9 were isolated from *Rauvolfia weddelianna* (our unpublished data). The names of the alkaloids are as follows: 1, indolo[2,3-*a*]quinolizine-2-ethanol, 1,2,3,4,6,7,12,12b-octahydro-9-hydroxy-β-vinyl; 2, indolo[2,3-*a*]quinolizine-2-ethanol, β-ethenyl-1,2,3,4,6,7,12,12b-octahydro-9-hydroxy-, 5-oxide; 3, strictosamide; 4, cyclopentanol, 3-ethenyl-1,-methyl-2-(5-methoxy-9*H*-pyrido[4,3-*b*]indol-4-yl); 5, cyclopentanol, 3-ethenyl-1,-methyl-2-(5, 7-dimethoxy-9*H*-pyrido[4,3-*b*]indol-4-yl); 6, 18-norajmalan-17,19-diol, 1,2-didehydro-1-demethyl-21-methyl-, 17-acetate; 7, Sarpagan-17-ol, 10-methoxy-; 8, reserpine; yohimban-16-carboxylic acid, 11,17-dimethoxy-18-[(3,4,5-trimethoxybenzoyl)oxy]-, methyl ester; and 9, yohimban-16-carboxylic acid, 17-hydroxy-, methyl ester.

Recombinant *Pb*MLS. Recombinant *Pb*MLS (*Pb*MLSr) was obtained as described by Neto et al. (3). Briefly, the cDNA encoding *Pb*MLS was inserted in the pET-32a(+) expression vector (Novagen, Madison, WI, USA). The resulting plasmid was transferred to *E. coli* strain BL21 C41(DE3). His-tagged *Pb*MLSr was purified using the nickel-nitrilotriacetic acid (Ni-NTA) spin kit (Qiagen, Germantown, MD, USA), and the tags were subsequently removed by adding EKMax enterokinase (Invitrogen, Carlsbad, CA, USA).

***Pb*MLSr activity assay in a microplate and screening for inhibitors.** The activity assays were performed as described previously by Roucourt et al. (29) and Zambuzzi-Carvalho et al. (2), with some modifications. Briefly, these assays were performed with an endpoint assay to measure the amount of acetyl coenzyme A (acetyl-CoA). The amount of free thiol groups of acetyl-CoA was determined using 5,5′-dithiobis-(2-nitrobenzoic acid) (DTNB) (Sigma, St. Louis, MO, USA) (30). The absorption at 415 nm was measured using a microplate reader model 680 (Bio-Rad Laboratories, Hercules, CA, USA). DTNB was added to a final concentration of 2 mM. The addition of DTNB to the mixture arrested the overall reaction due to the reaction of DTNB with the free thiol groups of cysteine (31). The standard reaction mixture contained 2 μg of *Pb*MLSr, 100 mM Tris-HCl, 5 mM $MgCl_2$, 2 mM glyoxylate (Sigma), and 1 mM acetyl-CoA (Sigma).

Pyruvic acid and the alkaloids were added at a concentration of 17 μg/ml as a positive control and to assess the inhibitory potential, respectively. The reaction mixtures were incubated for 30 min at pH 7.5. The specific activities were given in units per microliter of protein. Concen-

trations of the alkaloid compounds ranging from 6 to 36 μg/ml were tested (data not shown) to find the concentration that inhibited *Pb*MLS activity. All of the experiments were conducted in triplicate.

MICs. *Paracoccidioides brasiliensis* strain 18 (*Pb*18) yeast cells were cultivated on Fava-Netto's medium (1.0% [wt/vol] peptone, 0.5% [wt/vol] yeast extract, 0.3% [wt/vol] proteose peptone, 0.5% [wt/vol] beef extract, 0.5% [wt/vol] NaCl, 4% [wt/vol] glucose, and 1.4% [wt/vol] agar [pH 7.2]) (32) for 7 days at 36°C.

The method in CLSI M27-A3 (33) is not available for use with dimorphic fungi, such as those of the *Paracoccidioides* genus. So, in this study, to determine the MIC and to evaluate the growth of *Pb*18 yeast cells, we chose to use the standard method described by de Paula e Silva et al. (34), which is a colorimetric method based on document M27-A3 (33) but with adaptations and the addition of alamarBlue (BioSource, Carlsbad, CA, USA).

Inocula were prepared in RPMI 1640 (Invitrogen, Carlsbad, CA, USA) with L-glutamine, without sodium bicarbonate, supplemented with 2% glucose, and buffered to pH 7.0 using 0.165 M morpholinepropanesulfonic acid (MOPS) (Sigma, St. Louis, MO, USA). The *Pb*18 yeast cell suspension was adjusted to a final concentration in the range of 0.5×10^3 to 2.5×10^3 cells/ml in RPMI 1640. In the 96-well plates, the compounds were added in serial dilutions at concentrations ranging from 6 μg/ml to 300 μg/ml. The plates were incubated at 36°C and 150 rpm for 48 h. After this period, alamarBlue (BioSource) was employed, according to the manufacturer's instructions, and the plates were incubated for an additional 24 h for a total of 72 h prior to the final MIC reading. The lowest antifungal agent concentration that substantially inhibited the growth of the organism was visually determined at the point at which there was no change in the original blue color of the reagent.

Ligand affinity assays. Far-Western blot assays were carried out as previously described (3). *Pb*MLSr was subjected to SDS-PAGE and blotted onto a nylon membrane. After blocking for 4 h with 1.5% bovine serum albumin (BSA) in 10 mM phosphate-buffered saline (PBS)-skim milk and washing three times (for 10 min each time) in 10 mM Triton X-100 in PBS (PBS-T), the membranes were incubated with 20 μg/ml fibronectin or 30 μg/ml type I and IV collagen diluted in PBS-T with 2% BSA for 90 min and then washed three times (for 10 min each time) in PBS-T. Each compound was added at a concentration of 60 μg/ml. The membranes were incubated for 18 h with rabbit anti-fibronectin, anti-type I collagen, or anti-type IV collagen antibodies in PBS-T with 2% BSA (diluted 1:100). The blots were washed with PBS-T and incubated with peroxidase-labeled goat anti-rabbit immunoglobulin (diluted 1:1,000). The blots were washed with PBS-T, and the reactive signals were developed with hydrogen peroxide and diaminobenzidine (Sigma, St. Louis, MO, USA) as the chromogenic reagent. The positive control was obtained by incubating *Pb*MLSr with the polyclonal anti-*Pb*MLSr antibody (diluted 1:500), and the reaction was developed as described above.

ELISA. Enzyme-linked immunosorbent assay (ELISA) was carried out as described by Neto et al. (3). Briefly, polypropylene 96-well microtiter ELISA plates were sensitized with 10 μg/ml extracellular matrix (ECM) proteins overnight at 4°C and then blocked with 2% BSA, 10% fetal bovine serum (FBS), and 1% skim milk. To analyze the percentage of the inhibition of the adhesion of *Pb*18 yeast cells to the ECM by the tested compounds, each compound was added separately at a concentration of 60 μg/ml, and the mixture was incubated for 60 min. A total of 10^6 cells/ml of *Pb*18 yeast cells were added and incubated for 16 h at 37°C. To analyze the percentage of the inhibition of the adhesion of *Pb*MLSr to the ECM (ratio 1:1; 5 μg each), *Pb*MLSr and each compound at a concentration of 60 μg/ml was separately added to the plate. The percent inhibition of *Pb*MLSr and *Pb*18 yeast cell adhesion to the ECM by the tested compounds was calculated.

The reaction was developed using buffer citrate at pH 4.9 conjugated with *o*-phenylenediamine as the chromogenic substrate. Negative controls were performed using *Pb*MLSr or ECM only. The positive controls were performed using anti-*Pb*MLSr, anti-fibronectin, anti-type I collagen, or anti-type IV collagen antibody. The absorbance at 490 nm was measured, and the results were analyzed using the MicroCal Origin software version 5.0 (35).

Adhesion assays and fluorescence microscopy by IN Cell. The A549 and MRC5 cell lines were used for adhesion assays to evaluate the pattern of adherence of *Pb*MLSr and *Pb*18 yeast cells, as described by Mendes-Giannini et al. (36). A549 is a human lung adenocarcinoma cell line obtained from the American Type Culture Collection (Rockville, MD). These cells were cultured in Ham's F-12 medium supplemented with 10% heat-inactivated fetal calf serum. The MRC5 cell line was developed from lung tissue, and the cell morphology is fibroblast-like. These cells were cultured in Dulbecco's modified Eagle's medium (DMEM) (Gibco) supplemented with 10% heat-inactivated fetal calf serum. The cells were grown in 75-mm^3 bottles (Corning) and maintained at 36.5°C.

After 3 to 4 days, the cell line monolayer formed was trypsinized, and 96-well cell plates were prepared with 5×10^4 cells/ml. Briefly, the cell monolayer was washed with 1 ml of 0.2% trypsin solution and 0.02% Versene (ATV), and then 1 ml of ATV was added. In the following 1 to 2 min, the cells were mixed with various amounts of their corresponding medium plus 10% FBS. At this stage, the trypsin was neutralized by the 10% FBS present in the culture medium. The total volume of the cell suspension obtained was transferred to new bottles to obtain cell concentrations of 10^6 cells/ml. The cells were subcultured 2 days in advance. This procedure included trypsinization with 2 ml of ATV and the addition of 20 ml of culture medium. Five hundred microliters of this mixture was placed on coverslips in each well of a 24-well plate (5×10^4 cells/well).

A concentration of 60 μg/ml each compound was added per well. After adjusting the *Pb*18 yeast cell inoculum (1×10^6 to 5×10^6 cells/ml), the infection was performed for 15 h. For the *Pb*MLSr assays, a concentration of 5 μg/ml each compound was used. The controls containing *Pb*18 yeast cell inoculum (1×10^6 to 5×10^6 cells/ml) or *Pb*MLS without addition of the compounds were developed. Initially, the old medium was removed from the wells containing the cell line monolayer, and 100 μl of fresh medium was added to each corresponding plate well and then incubated at 37°C for 2 h. The infected plates were washed three times with PBS, fixed with 500 μl of 4% *p*-formaldehyde, and incubated overnight at 4°C.

To perform the indirect immunofluorescence assay, the fixed cells were permeabilized with 0.25% Triton X-100 in PBS (PBS-T) and incubated at room temperature for 30 min. After washing with PBS-T, cells were incubated with blocking solution (2.5% BSA, 1% skim milk, 8% fetal bovine serum) for 30 min at room temperature. After that, the blocking solution was discarded, and polyclonal anti-*Paracoccidioides* antibody (1:100) in blocking solution was added and incubated at 37°C for 1 h. After washing with PBS-T, the monolayer of cells was incubated with secondary antibody anti-rabbit IgG conjugated with Alexa 594-conjugated antibody (1:400) at 37°C for 1 h. Following, the ECM was labeled with anti-fibronectin or anti-collagen I or IV antibody (1:100) at 37°C for 1 h. After washing with PBS-T, the monolayer was incubated with anti-rabbit IgG conjugated with Alexa 594-conjugated antibody (1:400) at 37°C for 1 h. Finally, the monolayer was again washed with PBS-T, and 100 μl of 0.5 μg/ml 4′,6-diamidino-2-phenylindole (DAPI) was added for incubation at 37°C for 1 h. After successive washings with PBS-T, the reaction was fixed with 1% *p*-formaldehyde.

The potential fungal infection was observed using images processed by the IN Cell Analyzer 2000 system (GE Healthcare). All of the nuclei were stained with DAPI, and the actin filaments were revealed with phalloidin-fluorescein isothiocyanate (FITC). *Pb*18 yeast cells and *Pb*MLSr were detected with an Alexa 594-conjugated antibody. All experiments were repeated at least three times. The results were processed by means of fluorescence intensity by using the IN Cell Investigator software and statistically analyzed with Origin lab 7.5 software. The data were evaluated using one-way analysis of variance (ANOVA), followed by Tukey's test. A P value of <0.05 was considered significant.

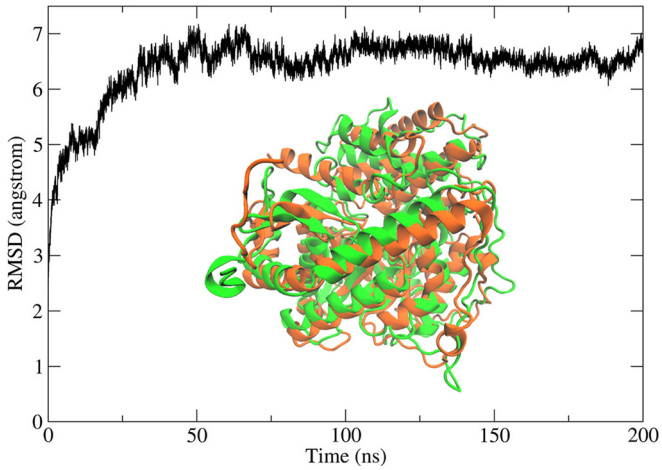

FIG 1 RMSD dynamic profile obtained for the MD simulations of *Pb*MLS over 200 ns. The homology model (orange) and the MD structure (green) of *Pb*MLS are superimposed in the ribbon model.

Cell cytotoxicity assay. The cell cytotoxicity assay was performed according to Mosmann (37). The cytotoxicity of the alkaloids for the A549 and MRC5 cell lines was assessed using the tetrazolium salt reduction (MTT) [3-(4,5-dimethylthiazol-2-yl)-2,5-diphenyltetrazolium bromide] method. The cells were grown in Ham's F-12 medium supplemented with 10% heat-inactivated fetal calf serum to A549 cells and DMEM (Gibco) supplemented with 10% heat-inactivated fetal calf serum to MRC-5 cells and maintained at 36.5°C. Concentrations ranging from 2.5 to 5.0 × 10^4 cells/ml were used for the formation of monolayer cells. The compounds, at concentrations ranging from 12 μg/ml to 600 μg/ml, were maintained in contact with the cells for 24 h. The cells were then treated with 5 mg/ml MTT reagent (Sigma, St. Louis, MO, USA) and incubated for 4 h. After the formation of formazan crystals, 100 μl of isopropanol was added to solubilize the precipitate, and the result was determined by the change in the color of the medium. The absorbance of formazan was quantified through an enzyme-linked immunosorbent assay using an ELISA reader set at 560 nm. Hydrogen peroxide was used as a positive control. The selectivity index (SI) values were calculated using the ratio of the 50% inhibitory concentration (IC_{50}) of the mammalian cells to the IC_{50} of the fungus.

RESULTS

***Pb*MLS structure.** The 3D homology model was built using the I-TASSER server based on the 3D structures of *E. coli* and *B. anthracis* malate synthase A, which had 49% identity to *Pb*MLS. The Ramachandran plot of the homology model had 92% of residues with Φ and ψ distribution in the favored region and 5% in the allowed regions. The quality factor of this structure was estimated to be 39.548 by Errat. This structure was then subjected to 200-ns MD simulations using the Gromacs program to achieve a stable structure according to the root mean square deviation (RMSD) for the nonhydrogen atoms. Figure 1 shows that the conformation of *Pb*MLS remained stable at an RMSD value of approximately 6.5 Å after approximately 100 ns of simulation. A cluster analysis of the conformations with a cutoff of 3 Å allowed the identification of seven conformations capable of representing the flexibility of *Pb*MLS for the full trajectory. The transient stability of *Pb*MLS suggested the presence of multiple ensembles in this structure. However, even under transient stability, after approximately 80 ns, only one of them effectively represented the trajectory (see Fig. S2 in the supplemental material). This conformation (cluster 1) was then used to perform molecular docking analysis.

Molecular docking with acetyl-CoA. Molecular docking simulations between *Pb*MLS and acetyl-CoA were performed to verify which amino acids are considered more important for the stability of acetyl-CoA. The results of this analysis were crucial for the identification of ligands capable of forming contacts corresponding to those expected with acetyl-CoA and decipher the mechanism of interaction with *Pb*MLS.

Figure 2 shows the key residues that provided stability to acetyl-CoA. The conformation shown in this figure corresponds to that of a lower energy and a higher incidence from the total of 1,000 independent simulations. The energy in this state was −18.0 kcal/mol, and this value was found in 21% of the simulations (see Fig. 3). All of the conformational modes that achieved success rates of >10% had energies between −17.8 and −18.3 kcal/mol. Acetyl-CoA had a total of 20 torsions to fit the *Pb*MLS binding pocket. The majority of the torsions were distributed along the main axis of the acetyl-CoA, and two of them were present between the rings and binding of a phosphate group.

It was possible to identify two distinct regions of acetyl-CoA interacting with *Pb*MLS: (i) a purine ring and (ii) an open-chain moiety. The region of the rings was completely buried in the cavity, forming polar and nonpolar contacts. In contrast, in the open-chain region, there was a greater number of polar contacts, but this region forms nonpolar contacts with Ile443, Tyr430, and Ile441. Side-chain H-bonds were observed between phosphate groups of acetyl-CoA and Lys217, Lys287, and Lys288. The variation of its ASA was 540 $Å^2$.

Virtual screening. (i) Classification by affinity criteria. Virtual screening using the ZINC database was performed to search for compounds binding to *Pb*MLS. In all simulations, the conformation of the compounds was limited to a region surrounding the main binding pockets of the protein. This region was defined according to the classification of DoGSiteScorer, considering only the larger volume cavity. All of these regions were then covered by the defined grid to limit the region of the conformational search. A total of 21 pockets were found, all of which had volumes covered by the considered grid. The binding pocket with the highest volume found by DoGSiteScorer was 4,492 $Å^3$, whereas the other volumes were <715 $Å^3$. The main binding pocket of *Pb*MLS had approximately 160 hydrophobic contacts, which represents approximately 31% of the relative number of hydrophobic site interaction centers (SIACs). In this pocket, we found 48% hydrophobic, 28% polar, 12% positive, and 12% negative contacts.

Figure S3 in the supplemental material shows the top 10 compounds selected based on the affinity criterion. The lowest energy values were −16.4 kcal/mol and −15.7 kcal/mol for compounds 8918338 (rank 2) and 12876659 (rank 1), which exhibited success rates of 91% and 98%, respectively (Fig. 3). The tenth-ranked compound was 8876676 (rank 10), which exhibited an energy value and success rate of −12.9 kcal/mol and 99%, respectively. In general, the success rate found for all of the compounds selected by the affinity criterion was >90%.

When the ligands were in the binding pocket of *Pb*MLS, the highest variation of ASA was found for compound 8876937 (412 $Å^2$) (rank 3). This same ligand was between two lower (by atom number)-ranked compounds based on the affinity criterion with only two torsions. Interestingly, ligand 8918302 (rank 6) had a success rate of 99% at finding the same energy, even if no torsion was available for its accommodation in the binding pocket.

Figure 4 shows how these ligands were accommodated in the

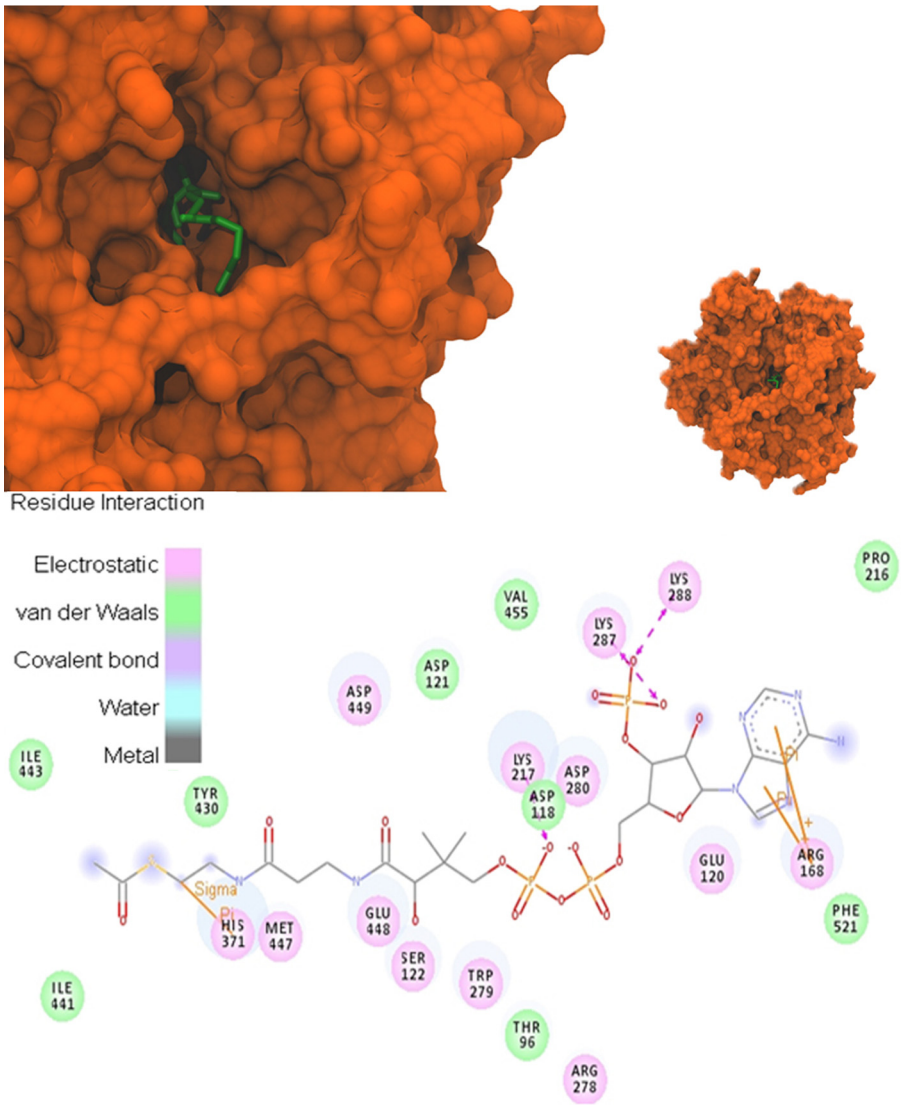

FIG 2 Molecular surface representation of the *Pb*MLS and LigPlots of the protein/acetyl-CoA in the binding pocket. The conformational structure of acetyl-CoA (green) refers to the lowest score obtained from the molecular docking simulations using AutoDock Vina.

binding pocket and which *Pb*MLS residues interacted more strongly with each ligand. Note that all of the ligands bound in the same pocket. Another important feature is the nature of the ligand contacts. The ligands had two well-defined regions, one with a high concentration of polar interactions (or H-bond contact), and another with a high concentration of nonpolar (van der Waals contact) interactions. This is a characteristic of amphipathic molecules that appears to be crucial for achieving stability in the pocket of *Pb*MLS. Nonpolar contacts with a higher occurrence were found for the Asp121, Trp279, and Thr96 residues. Similarly, the polar contacts had higher incidence in Arg168, His371, and Glu448. Note that the contacts did not necessarily indicate the nature of the residue but rather the type of contact that each residue formed with the ligands. In general, contacts involving Glu448, Ser122, His371, Asp449, Met447, and Thr96 were common in the interaction with *Pb*MLS, similarly to the interaction with acetyl-CoA. However, only the two best compounds selected based on the affinity criterion established contacts with the nonpolar residues Ile441 and Ile443 (Fig. 3 and 4).

(ii) Classification by efficiency criteria. Based on the efficiency criterion, the top 10 compounds were selected (Fig. 3; see also Fig. S4 in the supplemental material). The efficiency criterion selected ligands with low numbers of atoms and low affinity. These ligands were smaller in size than the other ranked ligands, with approximately half of the number of atoms. In general, it was verified that such compounds had contacts with several key residues of *Pb*MLS that interacted with acetyl-CoA. However, because they were smaller, most of the residues were located inside the cavity and preferably stabilized by nonpolar contacts (Fig. 3 and 5).

This feature found in the compounds screened resulted in chemical groups with high spatial complementarity in the binding pocket of *Pb*MLS; thus, the hydrogen bonds were not favored and observed in such compounds. As shown in Fig. 5, the top two compounds were accommodated in the binding pocket. Note that

	Rank	Compounds	Active torsions	Number of atoms[1]	ADVina score[2] (Kcal/mol)	ADVina energy[3] (Kcal/mol)	c[4]	dASA[5] (Å²)	Key Residues to Acetyl-CoA: GLU 120	SER 122	ARG 168	LYS 217	ARG 278	TRP 279	ASP 280	LYS 287	LYS 288	HIS 371	MET 447	GLU 448	ASP 449	THR 96	ASP 118	ASP 121	PRO 216	TYR 430	ILE 441	ILE 443	VAL 455	PHE 521	Common residues to Acetyl-CoA	Nonpolar contacts (nn)	Polar contacts (np)	Cv = (nn -np) / np
		Acetyl-CoA	20	51	-8,3	-18,0	0,21	540 (539)			PI							PI												-	9	11	-0,18
Affinity Criterion	1	12876659	5	41	-12,1	-15,7	0.98	301 (542[a])			PI								HB											11	4	7	-0,4
	2	8918338	6	40	-12,1	-16,4	0.91	308 (516)		HS																				9	3	6	-0,5
	3	8876937	2	38	-12,0	-13,4	0.91	412 (331)				HS								PI										12	8	4	1,0
	4	8790277	4	41	-11,9	-14,7	0.94	288 (400)				PI																		9	7	2	2,5
	5	8876604	2	39	-11,8	-13,2	0.99	359 (328)				PI					PI													8	2	6	-0,7
	6	8918302	0	36	-11,8	-11,8	0,99	373 (292)			PI	PI	PI																	8	3	5	-0,4
	7	3848528	4	40	-11,8	-14,6	0,99	238 (490)		HS																				6	3	3	0,0
	8	8918516	5	39	-11,7	-15,1	0,96	291(545)			PI								HB											9	2	7	-0,7
	9	8876707	2	40	-11,6	-13,0	0,98	376 (329)				PI																		7	5	2	1,5
	10	8876676	2	39	-11,5	-12,9	0,99	371 (309)				PI																		10	7	3	1,3
Efficency Criterion	1	2097571	1	23	-9,5	-10,1	0.99	233 (272)																						7	4	3	0,3
	2	12658252	1	23	-9,5	-10,1	0.71	218 (300)			PI	PI	PI																	10	7	3	1,3
	3	4293427	0	23	-9,2	-9,2	0.94	221 (290)			PI																			9	1	8	-0,9
	4	12657531	2	23	-9,2	-10,3	1.00	226 (281)																						7	5	2	1,5
	5	4083620	1	21	-9,0	-9,5	1.00	230 (264)																						6	4	2	1,0
	6	12503788	0	21	-9,0	-9,0	1.00	214 (275)																						11	9	2	3,5
	7	13399111	0	21	-9,0	-9,0	0.97	239 (271)																						9	9	0	0,0
	8	13400190	2	20	-8,9	-9,9	0.95	211 (269)																						8	7	1	6,0
	9	13400661	0	20	-8,8	-8,8	1.00	208 (270)																						8	7	1	6,0
	10	3999192	0	20	-8,4	-8,4	1.00	190 (259)			PI		PI																	10	4	6	-0,3
Alkaloids	Inhibitors 8	8	10	46	-8,9	-14,1	0.76	488 (391)			PI		PI				PI													14	7	7	0,0
	Inhibitors 3	3	4	41	-10,6	-13,1	0.89	403 (364)		HS		PI							HB			HS								13	1	12	-0,9
	Inhibitors 4	4	4	27	-7,9	-9,8	0.88	298 (299)				PI																	PI	7	4	3	0,3
	Inhibitors 6	6	4	28	-8,4	-10,4	0.96	234 (329)					HS											HS						11	6	5	0,2
	non Inhibitors 9	9	3	29	-8,5	-10,0	0,98	276 (315)				PI																		8	3	6	-0,5
	non Inhibitors 1	1	5	27	-8,3	-10,7	0,69	253 (308)																						6	4	2	1,0
	non Inhibitors 2	2	6	28	-8,2	-11,1	0,83	250 (318)			PI																			12	3	9	-0,7
	non Inhibitors 7	7	4	26	-8,1	-10,0	0,87	236 (325)						HS																13	2	11	-0,8
	non Inhibitors 5	5	5	29	-7,6	-9,8	0.70	290 (329)				PI																		11	6	5	0,2
Rank Key Residues									6	15	24	19	17	19	11	3	9	13	15	26	8	19	9	22	5	0	2	3	7	7			

FIG 3 Scores and key residues of the compounds obtained in binding pocket of *Pb*MLS. Nonpolar contacts are represented in green, and polar contacts are represented in pink. CV, coefficient of variation between the number of nonpolar and polar residues in contact with acetyl-CoA; PI, π or σ interaction; HB, hydrogen bond with side chain; HS, hydrogen bond with backbone. Further information on the listed variables is indicated with superscript numbers, as follows: 1, number of atoms (except hydrogen atoms); 2, AutoDock Vina (ADVina) score obtained for mode-1 (lowest energy) used in the definition of the compound's rank; 3, AutoDock Vina energy is the term c_{inter} in equation 1 obtained for mode-1; 4, success rate in obtaining the same score in a total of 1,000 independent simulations; 5, dASA is the variation of the accessible surface area (ASA) to take the ligand in the binding pocket of *Pb*MLS; parentheses indicate the ASA to the solvent in the cavity of *Pb*MLS.

the Trp279, Glu448, and Asp121 residues could form contacts with almost all of the compounds ranked based on the efficiency criteria (Fig. 3). Most of the compounds were in a favorable position to interact with Arg168 through PI.

Of the 10 compounds ranked by efficiency, seven had more than eight contacts similar to those found with acetyl-CoA, regardless of the nature of the contact (polar or nonpolar). Compound 12503788 (rank 6) showed greater correspondence with nine nonpolar contacts and two polar contacts. Conversely, compound 4293427 (rank 3) resulted in eight polar contacts similar to those found for acetyl-CoA and only one nonpolar contact (Fig. 3).

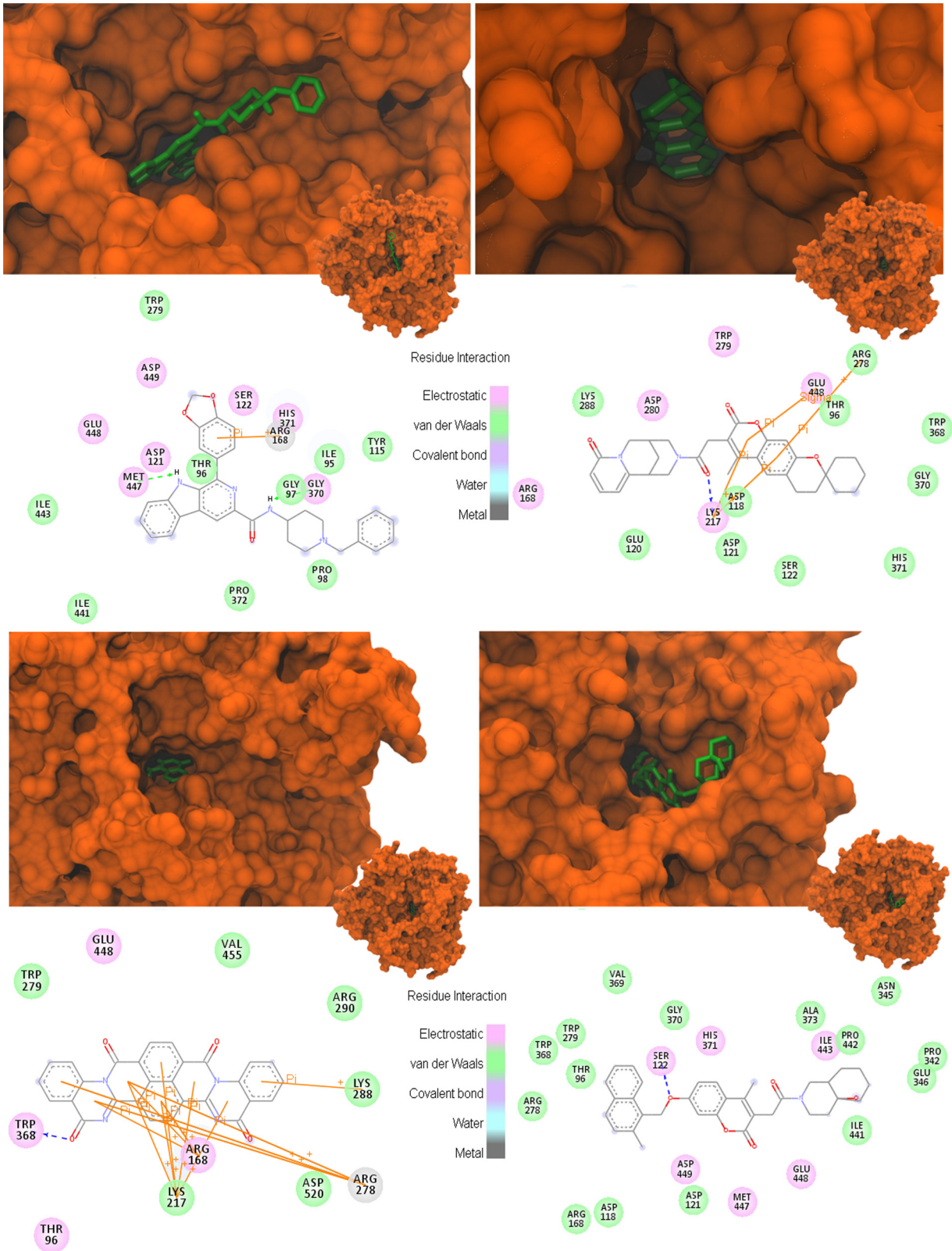

FIG 4 Molecular surface representation of *Pb*MLS and LigPlot diagrams of four compounds selected based on the affinity criterion. The modes of interaction for compounds 12876659 (top left), 8876937 (top right), 8918302 (bottom left), and 8918338 (bottom right) are shown in green. π-interactions are represented by orange lines, green dashed arrows indicate hydrogen-bond interactions with amino acid main chains, and blue dashed arrows indicate side-chain hydrogen-bond interactions. The arrowhead directs toward the electron donor. The structures of the compounds correspond to the lowest scores and the highest hits for a total of 1,000 independent simulations performed using AutoDock Vina.

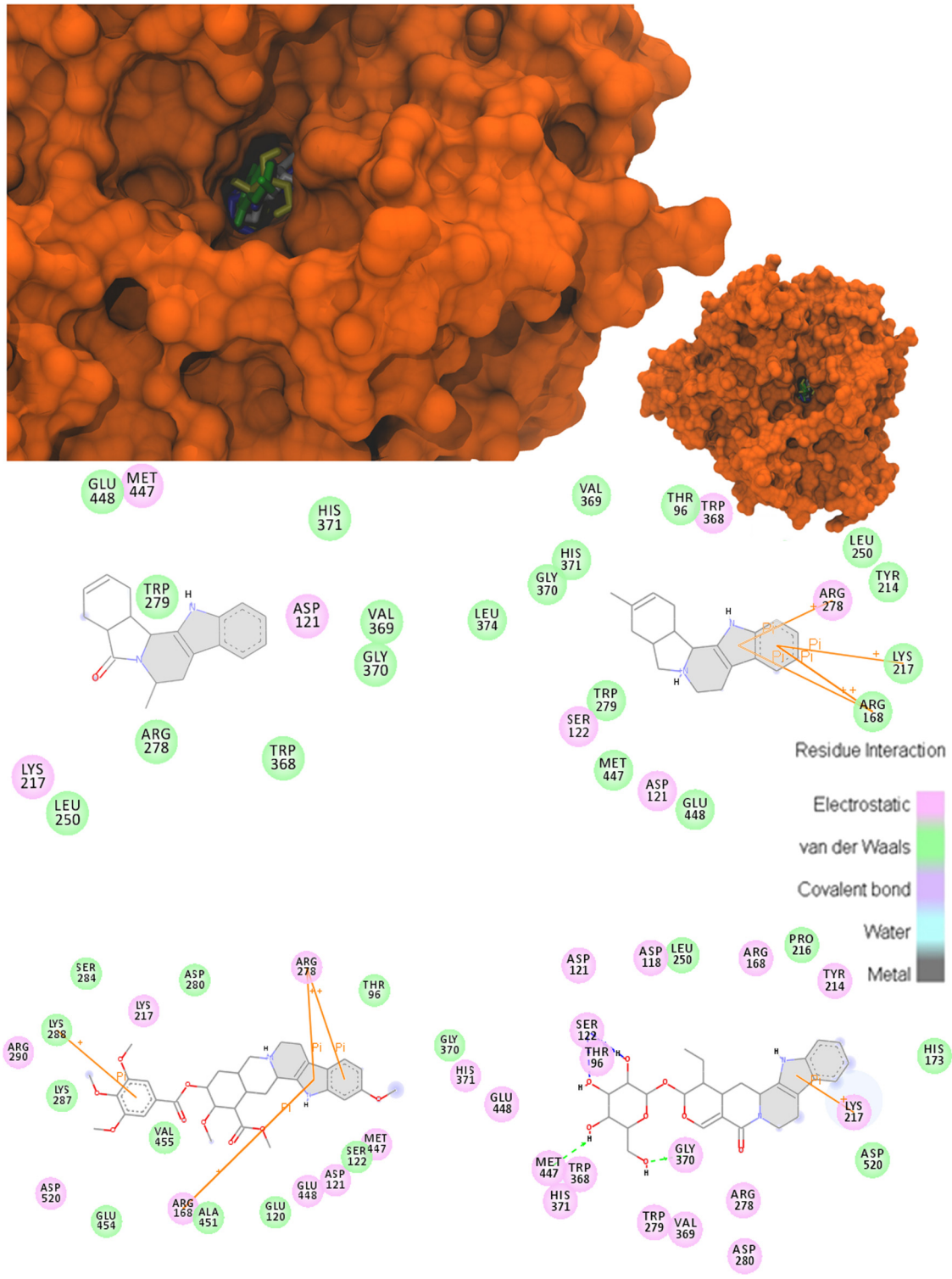

FIG 5 Molecular surface representation of *Pb*MLS and LigPlot diagrams of the top two compounds selected by the efficiency criterion and of the top two alkaloids that interfered with *Pb*MLSr activity and fungal growth. The modes of interaction of each of the following compound are shown: 2097571 (blue), 12658252 (white), alkaloid 8 (green), and alkaloid 3 (yellow). The LigPlots of compounds 2097571 (top left), 12658252 (top right), alkaloid 8 (bottom left), and alkaloid 3 (bottom right) are shown. π-interactions are represented by orange lines, green dashed arrows indicate hydrogen-bond interactions with amino acid main chains, and blue dashed arrows indicate side-chain hydrogen-bond interactions. The arrowhead directs toward the electron donor. The highlighted rings are common among the compounds. The structures of the compounds correspond to the lowest scores and highest hits from a total of 1,000 independent simulations using AutoDock Vina.

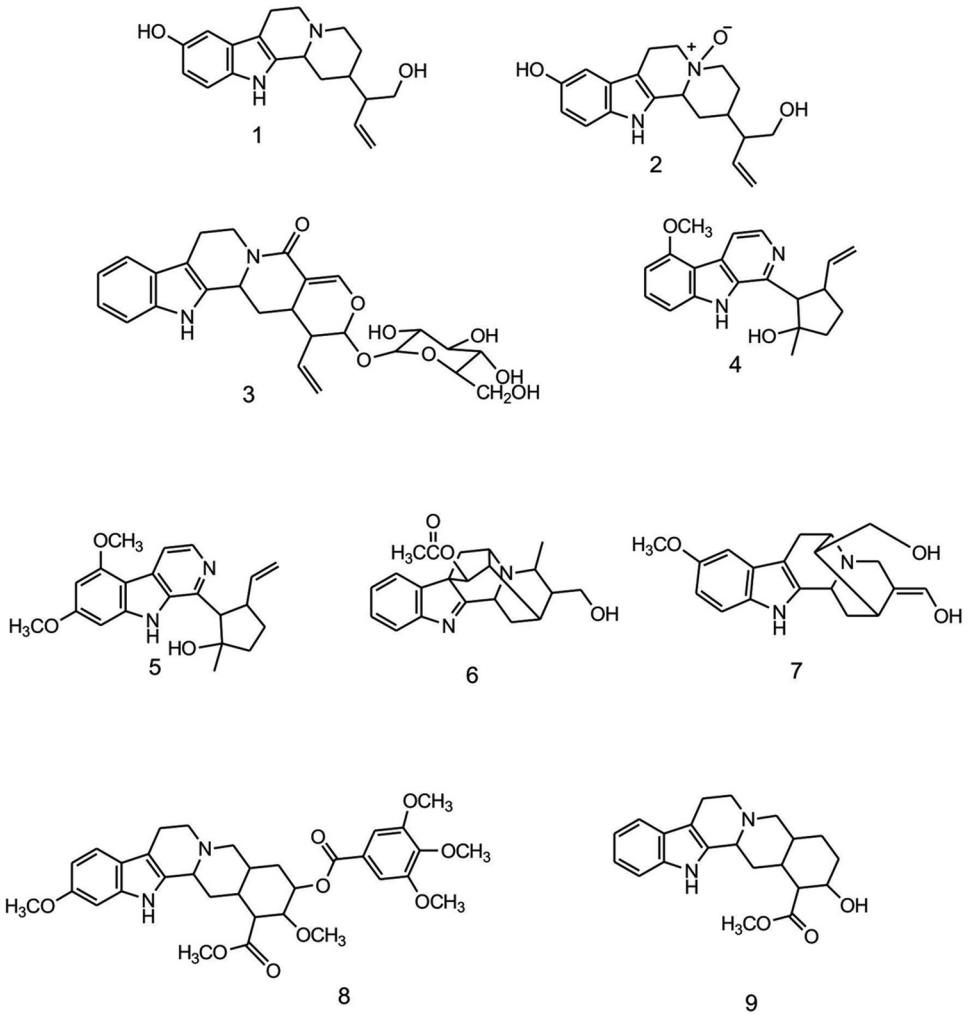

FIG 6 Structures of the nine selected alkaloids.

Molecular docking with alkaloids. Based on the top compounds ranked by affinity and efficiency parameters from virtual screening, we identified a topological pattern to understand the alkaloid indole moiety (highlighted in Fig. 5). Since these structural features and its angles were also present on a series of β-carboline alkaloids isolated by our research group from *Rubiaceae* and *Apocynaceae* species, they were introduced in this study (Fig. 6).

Molecular docking simulations were performed using AutoDock Vina for all alkaloids shown in Fig. 3, but only alkaloids 8 and 3 had known modes of interaction (Fig. 5). The affinities of these two alkaloids in the binding pocket are also shown in Fig. S5 and S6 in the supplemental material. The comparison of all of the alkaloids and acetyl-CoA is shown in Fig. 3. Alkaloids 8 and 3 had numbers of atoms similar to those found for acetyl-CoA. Note that alkaloids 8 and 3 had the lowest energies of interaction found for all of the alkaloids and, interestingly, had the same energy magnitude as the top-ranked compounds obtained by virtual screening. The top five highest-ranked compounds based on the affinity criterion had energies between −15.7 kcal/mol and −13.2 kcal/mol, whereas the energies of alkaloids 8 and 3 were −14.1 kcal/mol and −13.1 kcal/mol, respectively. The total number of atoms among these compounds was also very similar, i.e., approximately 40 atoms. With the exception of alkaloids 8 and 3, all of the other compounds had very similar energies. The success rates at achieving these energies were >70% for all of the alkaloids.

Even when the torsion effects were included in the AutoDock Vina scores, these two alkaloids had the lowest scores. The high number of torsions for alkaloid 8 (10 torsions) maintained its score (−8.9 kcal/mol) at a greater level than that of alkaloid 3 (−10.6 kcal/mol) but lower than that of all of the other alkaloids. All of them were located in the same region of the binding pocket of *Pb*MLS, making contacts with the Asp280 and Arg278 residues (Fig. 3).

The chemical groups of the amino acids involved in the interactions discussed above can be observed in Fig. S5 and S6 in the supplemental material.

The contacts involved in the interaction between acetyl-CoA and *Pb*MLS were also verified for each alkaloid. Note that alkaloid 8 had the highest incidence of contacts among all of the alkaloids and compounds ranked. None of the compounds ranked by the efficiency and affinity criteria resulted in an incidence of contacts close to those observed for acetyl-CoA. Alkaloids 3 and 2 had 13

TABLE 1 Inhibitory effect of alkaloid compounds on *Pb*18 growth and *Pb*MLS activity

Compound/ antifungal	*Pb*18		*Pb*MLS	
	IC_{50} (μg/ml)[a]	MIC (μg/ml)	IC_{50} (μg/ml)[b]	Specific activity (U[c]/μl)
8	46.21	62.02	17 ± 0.1	46.2 ± 0.1
3	160.36	249.50	29 ± 0.0	80.5 ± 0.1
6	135.87	249.57	21 ± 0.0	102.4 ± 0.1
4	4.04	8.76	17 ± 0.0	97.5 ± 0.3
9			NF[d]	515.5 ± 0.1
1			NF	512.0 ± 0.3
2			NF	501.0 ± 0.3
7			NF	518.3 ± 0.2
5			NF	488.4 ± 0.4
Itraconazole	0.01	0.015		
Amphotericin B	0.06	0.12		
Pyruvic acid			4.8 ± 0.0	104.5 ± 0.4
Control[e]			NF	521.7 ± 0.2

[a] IC_{50} for *Pb*18, concentration that inhibits 50% of cell growth, visualized by a decrease of 50% in absorbance compared to that of the control cell.
[b] IC_{50} for *Pb*MLS, concentration that inhibits 50% of enzyme activity, visualized by a decrease of 50% in absorbance compared to that of the control.
[c] One mole of coenzyme A formed per minute.
[d] NF, not found.
[e] Without compound and pyruvic acid.

contacts similar to those found for acetyl-CoA, but only alkaloid 3 had an energy score close to that of alkaloid 8.

Large amounts of H-bonds and PI were found for alkaloids 3 and 8. Alkaloid 8 had PI with Arg168, Arg278, and Lys288, and these were also found in the interaction with acetyl-CoA. Alkaloid 3 had three H-bond contacts with Ser122, Met447, and Thr96 and a PI with Lys217. All of these interactions were crucial for the stability of alkaloid 3, because the polar contacts were prevalent in approximately 92% of the contacts. Perhaps, for this reason, alkaloid 3 had a β-carboline unit slightly outside the cavity compared with the other compounds. Alkaloid 6 had 11 contacts in common with acetyl-CoA, and two of these involved H-bonds with Arg278 and Asp121.

Finally, the change in the ASA of the alkaloids was determined to evaluate their possible contributions to the free energy of solvation (not estimated here). As shown in Fig. 3, alkaloids 3 and 8 showed variations in the ASA of >50% than most of the other alkaloids. The ASA variation found for these two compounds was >400 Å^2. In the case of alkaloid 8, the variation in the ASA was >2-fold greater than that found for alkaloid 2. Changes in the ASA values of >400 Å^2 were found only for compound 8876937 (rank 3) and acetyl-CoA. This variation was relevant for the stability of the compounds, particularly when there are more nonpolar contacts than polar contacts.

Inhibitory effect of alkaloid compounds on *Pb*MLSr activity. The inhibition of *Pb*MLSr by alkaloid compounds was investigated. Concentrations of the alkaloid compounds ranging from 6 to 36 μg/ml were tested (data not shown) to find the concentration that inhibited *Pb*MLS activity. Of the nine compounds tested, four inhibited *Pb*MLSr. Compounds 3, 4, 6, and 8 inhibited *Pb*MLSr more effectively than the known inhibitor pyruvic acid. The inhibition with compound 8 was higher than that with compounds 3, 4, and 6 (Table 1).

Inhibitory effect of alkaloid compounds on *Paracoccidioides* species growth. This study verified that the alkaloid compounds that inhibited *Pb*MLSr can interfere with the growth of *Pb*18 yeast cells. The microplate microdilution assay using alamarBlue was performed to measure the viability of *Pb*18 yeast cells (34). Itraconazole and amphotericin B were used as positive controls. The results showed that alkaloids 4 and 8, which had lower MICs and IC_{50}s, were more effective at inhibiting fungal growth (Table 1).

Inhibition of the adhesion of *Pb*MLSr to ECM. Because *Pb*MLS is an anchorless adhesin and binds to fibronectin and type I and IV collagen, we investigated whether alkaloids 4, 8, 6, and 3 could prevent the adhesion of *Pb*MLSr to these ECM components through a far-Western blot assay. Alkaloids 4, 8, 6, and 3 inhibited the adhesion of *Pb*MLSr to fibronectin and type I and IV collagen (Fig. 7A, B, and C, respectively). A positive reaction was visualized to ECM bound to *Pb*MLSr immobilized in the membrane (Fig. 7A to C, line 5). The results showed that the alkaloid compounds inhibited *Pb*MLSr adhesion to these ECM components.

To validate the data described above, we investigated whether this process could also occur through an ELISA (Table 2). Thus, the ECM components were immobilized in the plate, and the alkaloid compounds and *Pb*MLSr were then added. Negative controls were performed using *Pb*MLSr or ECM only. Positive controls were performed using anti-*Pb*MLSr, anti-fibronectin, anti-type I collagen, or anti-type IV collagen antibody (data not shown). It was observed that alkaloids 3, 6, 4, and 8 inhibited the adhesion of *Pb*MLSr and *Pb*18 to fibronectin and type I and IV collagen. The analysis of all ECM components revealed that the

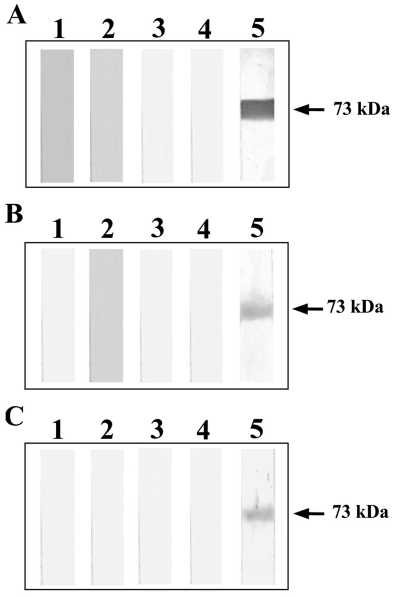

FIG 7 Binding of *Pb*MLSr to extracellular matrix components. *Pb*MLSr was subjected to SDS-PAGE and electroblotted. The negative control was obtained by incubating the *Pb*MLSr with peroxidase-conjugated anti-rabbit IgG (data not shown). The membranes were reacted with fibronectin and type I and IV collagen (A, B, and C, respectively), incubated with alkaloids 4 (lane 1), 8 (lane 2), 6 (lane 3), and 3 (lane 4), and subsequently incubated with rabbit IgG anti-laminin, anti-fibronectin, and mouse anti-type I and anti-type IV collagen antibodies, respectively. The positive control was obtained by incubating the recombinant protein with anti-*Pb*MLS polyclonal antibody (A, B, and C, lane 5). Peroxidase-conjugated anti-rabbit and anti-mouse IgG were used to reveal the reactions.

TABLE 2 Percent inhibition of the adherence of *Pb*MLSr and *Pb*18 to ECM by alkaloid compounds

Compound	% inhibition of adherence of *Pb*MLSr/*Pb*18 to ECM for:		
	Fibronectin	Type I collagen	Type IV collagen
4	19.60/30.0	27.59/33.98	21.38/34.63
8	25.93/5.05	33.03/12.59	21.62/14.36
6	18.88/5.27	37.17/31.45	19.47/34.31
3	41.10/8.51	31.52/9.18	17.79/12.64

inhibition of the adhesion of *Pb*MLSr by alkaloids 8 and 3 was higher than that obtained with *Pb*18. In contrast, the inhibition of the adhesion to *Pb*18 by alkaloid 4 was higher than that obtained with *Pb*MLSr. The analysis of fibronectin and type I collagen showed that the inhibition of the adhesion to *Pb*MLSr by alkaloid 6 was higher than that found with *Pb*18. The analysis of type IV collagen showed that the adhesion to *Pb*18 was higher than that to *Pb*MLSr.

Considering *Pb*MLSr, a higher inhibition was observed when fibronectin (to alkaloid 3 only) or type I collagen was used. Low inhibition by all alkaloids was observed with type IV collagen. Considering the fungus, higher inhibitions were observed in the adhesion to type I and IV collagen.

Fluorescence microscopy by IN Cell. The adhesion of *Pb*MLSr and *Pb*18 to A549 and MRC5 cells in the presence of alkaloid compounds was evaluated using IN Cell Analyzer 2000 system light microscopy (Fig. 8). The adhesion was investigated using the antibodies corresponding to ECM fibronectin, type I collagen, or type IV collagen. The markers phalloidin-FITC (green), DAPI (blue), and anti-*Paracoccidioides* polyclonal serum plus Alexa 594-conjugated antibody (red to yellow) were used to visualize actin filaments, nuclei, *Pb*18 yeast cells and *Pb*MLSr, respectively. The fluorescence staining of *Pb*MLSr and *Pb*18 adhered to cells, and the adhesion inhibition by the alkaloids to ECM was measured. A more intense red indicates a greater adhesion of *Pb*MLSr and *Pb*18 to the cells. The fluorescence staining intensity is shown

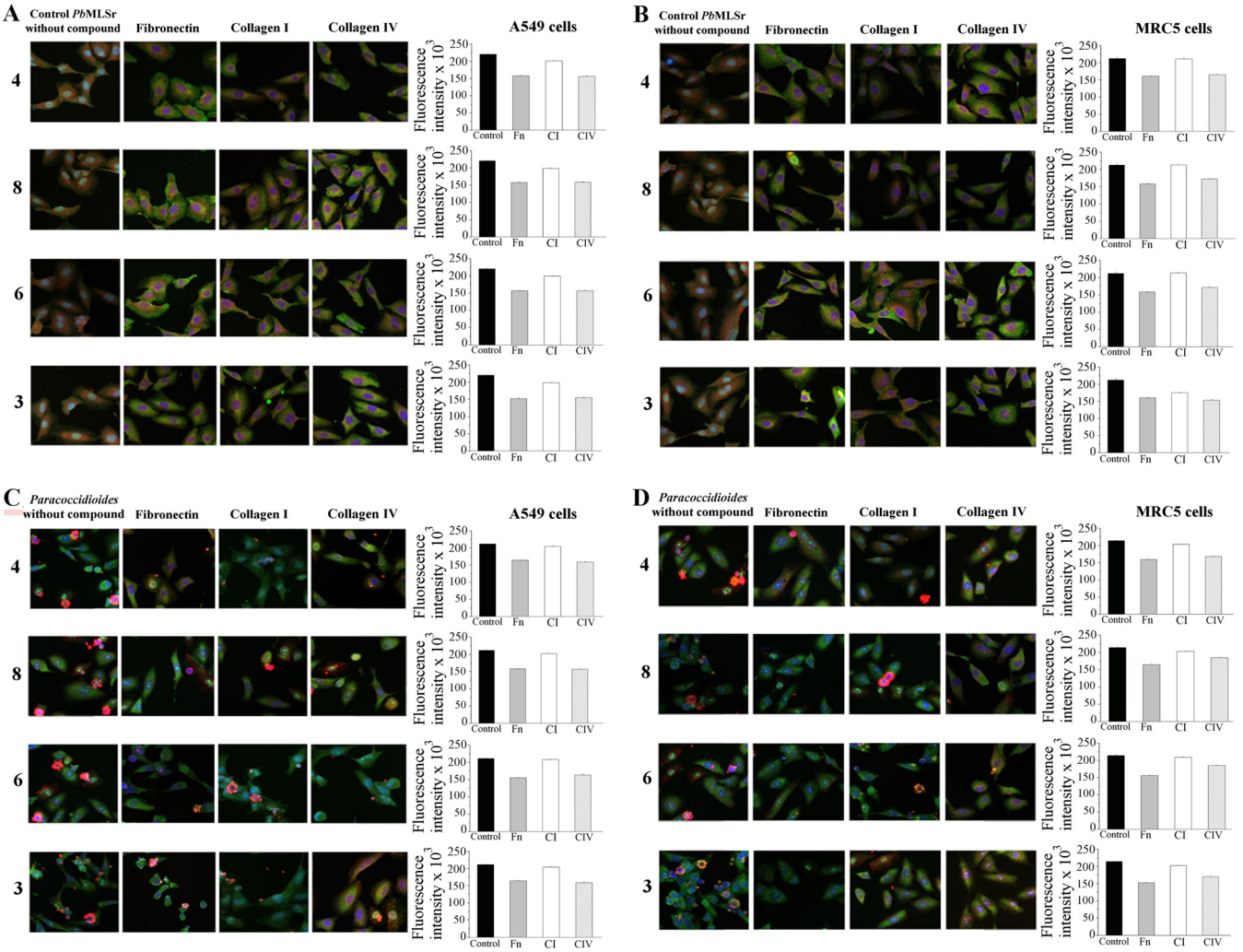

FIG 8 Inhibition of the adhesion of *Pb*MLSr and *Pb*18 to A549 and MRC5 cells. The inhibition of the adhesion of *Pb*MLSr to A549 (A) and MRC5 (B) cells and of *Pb*18 to A549 (C) and MRC5 (D) cells by the alkaloid compounds was evaluated after 2 h of incubation. Green, phalloidin-FITC; blue, DAPI; red to yellow, anti-*Paracoccidioides* sp. polyclonal serum plus Alexa 594-conjugated antibody. The fluorescence staining intensity is shown in the graphs. The assays were conducted using an IN Cell Analyzer 2000 using light microscopy.

TABLE 3 Cytotoxic effect of alkaloid compounds

Compound	IC_{50}s ± SD (μg/ml)[a]		Selective toxicity index	
	A549	MRC5	A549	MRC5
4	225 ± 0.3	273 ± 0.4	55.7	67.6
8	170 ± 0.4	249 ± 0.6	3.7	5.4
6	49 ± 0.5	268 ± 0.7	0.4	2.0
3	202 ± 0.4	235 ± 0.3	1.3	1.5

[a] IC_{50}, concentration that inhibits 50% of cell growth, visualized by a decrease of 50% in absorbance compared to that of the control cell.

in Fig. 8. The results showed that all four compounds inhibited the adhesion of *Pb*MLSr to A549 (Fig. 8A) and MRC5 (Fig. 8B) cells. The four compounds also inhibited the adhesion of *Pb*18 to A549 (Fig. 8C) and MRC5 (Fig. 8D) cells. The inhibition of adhesion was higher to fibronectin and type IV collagen than to type I collagen, considering *Pb*MLSr, *Pb*18, or type of cells (Fig. 8). In contrast, the ELISA results showed that the inhibition of adhesion was higher to type I collagen (Table 2). The small differences between the results may be due to differences in the principles of the techniques.

Cell cytotoxicity assay. The cytotoxic effect of alkaloids 4, 8, 6, and 3 was investigated in A549 and MRC5 cells through an MTT assay. The results showed that the alkaloid compounds were generally not cytotoxic to MRC5 and A549 cells at the concentrations used to inhibit *Pb*MLSr activity and *Pb*18 growth or in the adhesion experiments (Table 3). Only alkaloid 6 was cytotoxic to A549 cells, as determined based on the MIC to *Pb*18 growth (Table 1). The selective toxicity index to each compound was calculated. The higher index values were found to compounds 4 and 8 (Table 3).

DISCUSSION

There were two distinct regions of acetyl-CoA that interacted differently with *Pb*MLS. One of the regions, the purine ring, was completely buried in *Pb*MLS. Only one torsion was found between the purine ring and the adjacent cycle, conferring specificity to this region and thus favoring binding to the internal region of the binding pocket by complementarity (see Fig. 2). The other region, the open-chain moiety, is projected out of the *Pb*MLS cavity. This region interacts with nine critical amino acid residues of *Pb*MLS by forming nonpolar contacts (see Fig. 3). It has several degrees of freedom, approximately 18 torsions, which provide flexibility to accommodate its poor nonpolar content through contacts that minimize the area exposed to the solvent. In this case, nonpolar contacts with Ile443 and Ile441 were favored at the entrance of the cavity. This region of acetyl-CoA was not critical for providing specificity to *Pb*MLS, because its polar content may be available to the solvent. However, based on these findings, the pocket of *Pb*MLS was concentrated in the innermost region of the molecule and had a large volume, indicating that these polar interactions were important for ensuring that acetyl-CoA has initial stability in the main entrance of the cavity of *Pb*MLS. In addition, the surface complementarity generated by the rings provided sufficient stability to ensure that acetyl-CoA was not carried to the solvent but rather was partially fixed in the cavity. Therefore, the interaction of acetyl-CoA in this region may be important for inhibiting the interaction of *Pb*MLS to other molecules by surface complementarity. As shown in Fig. 1, the coefficient of variation (CV) for each compound was presented to measure the balance between the polar and nonpolar contacts compared with those found for acetyl-CoA. The CV for acetyl-CoA was only −0.2, suggesting that there was a balance between the contributions and therefore indicating that the amphipathic nature of acetyl-CoA may be critical for ensuring stability in the *Pb*MLS binding pocket.

The selection based on the affinity and efficiency criteria was essential for providing new compounds with greater complementarity to *Pb*MLS. Most of these compounds presented a common structural pattern, namely, the β-carboline moiety, which was crucial for the binding to *Pb*MLS. In addition, they presented a region capable of performing polar contacts. Acetyl-CoA also bound to *Pb*MLS through the purine ring portion, which is very similar to the indole moiety in the β-carboline alkaloids.

Although all of the alkaloids shown in Fig. 6 are β-carboline-type alkaloids, some of them do not have a polar group (hydroxyl or methoxyl) in the indole portion. The presence of a β-carboline moiety and of hydroxyl and methoxyl groups forming polar contacts were likely the main differences observed in the inhibitory power of compounds 8 and 3 in relation to the others. In the case of alkaloid 3, none of these polar groups was found to be present in the β-carboline group, resulting in a group with more hydrophobic (or less polar) content than that of the others. Additionally, with the exception of alkaloid 3, all of the compounds capable of inhibiting *Pb*MLS and the fungus had CVs of <0.3. Alkaloid 8, which had a higher ability to inhibit *Pb*MLS and the fungus, exhibited the lowest energy of all the alkaloids, which was similar to that found for acetyl-CoA. However, two other measures could also help distinguish this compound from the others: (i) the greatest variation in the ASA and (ii) a CV of 0. These measures indicate that it has amphipathic characteristics similar to those found in acetyl-CoA.

Although most polar interactions contribute to the stability of the compounds, we believe that the variation in the ASA is the most important to ensure the stability of the compounds. When nonpolar groups are exposed to solvent, they were rapidly driven into the cavity of *Pb*MLS to ensure their protection from the solvent. This action was a collective result of the solvent molecules, which provided a significant gain in the entropy of the system, favoring the reduction of the free energy of binding. Such contributions were estimated by the binding energy of AutoDock Vina through a distance-dependent term, which considered only the interaction between hydrophobic atoms. This is a way to include the contributions to the free energy of solvation. Therefore, measures of the variation in the ASA determined in this study were slightly correlated with measures of the energy determined by AutoDock Vina ($r = 0.7$). We believe that the variation in the ASA of the compounds studied here shows the importance of minimizing the exposure of nonpolar groups from compounds or of maximizing the entropy of the medium. The advantage of this type of contribution is that the lowest energy states were more rapidly accessed than those prevented kinetically by frustrated states (polar contacts).

In the particular case of alkaloid 3, which had a low CV of −0.9, we believe that the unbalance between the contributions of nonpolar and polar contacts may have been offset by H-bonds and PI with the amino acid residues of *Pb*MLS. This ensured ≥13 contacts similar to those observed with acetyl-CoA but an unbalance in relation to the nature of the contacts. In any case, its inhibitory

power was approximately 2-fold lower than that observed for alkaloid 8.

Finally, the comparison of alkaloids 5 and 4 revealed that the first compound was unable to inhibit *Pb*MLS and fungal growth. Our interpretation of this marked difference is not easily understood by the parameters shown in Fig. 3. We understand that there is a very fine energy threshold involving the stability of alkaloids 5 and 4 in the binding pocket of *Pb*MLS. The structural difference between these two compounds was only one methoxyl group in favor of alkaloid 5. Both compounds were able to establish contact with the nonpolar residues, such as Val455 and Phe521, which were located within the binding pocket of *Pb*MLS. This is a region that is favorable for the formation of nonpolar contacts, which were critical for the stability of these alkaloids.

In addition, polar contacts with Glu120, Arg168, and Lys217 also occurred in both alkaloids. All of these contacts were also present in the interaction between *Pb*MLS and acetyl-CoA. Note that these two alkaloids (4 and 5) are smaller than acetyl-CoA and the other highest-scoring alkaloids studied here. Therefore, the difference between these two alkaloids and acetyl-CoA seems to be related to the number of contacts and the nature of the contacts, which might be critical. Thus, if we consider the total number of contacts found for the two alkaloids, which were common to those found for acetyl-CoA, alkaloid 5 had 36% (4/11) of its contacts frustrated in relation to acetyl-CoA; those contacts that should be polar were formed by nonpolar contacts, and vice versa. The analysis of alkaloid 4 showed that only 14% (1/7) of the contacts differed. This is a crude attempt to understand the differences between these two compounds. However, all of these hypotheses should be checked to estimate the ligand dissociation path to calculate the smooth reaction path that links the bound and unbound states. In our next study, these estimates should be determined using umbrella sampling to calculate the mean force potential and to estimate the binding free energy of each alkaloid.

The selective toxicity index of ≥5- or 10-fold, more selective for A549 and MRC5 cell lines than for the fungus, is typically expected for new antimicrobials. The higher indexes were found to compounds 4 and 8, mainly considering MRC5, which are healthy cells. This find indicates the good features of these compounds. The inhibitory effect of alkaloids on *Paracoccidioides* species growth was performed with only one strain, since the compounds have been extracted from plants in small amounts. More assays with other strains should be done; however, the phytochemical methodology for isolation of the alkaloids must be repeated. This procedure comprises plant collection in the flowering season, December to February, chromatographic separation and purification, and spectroscopic analysis of the compounds (26–28).

Our group has shown that the exposure of *Paracoccidioides* spp. to the natural product oenothein B results in changes in the transcriptional profile, level of cell wall polymers, and yeast cell morphology (38, 39). We also searched for inhibitors to the isocitrate lyase from the glyoxylate cycle of *Paracoccidioides* species (*Pb*ICL). This study reports on the inhibitory action of argentilactone and its derivatives on *Paracoccidioides lutzii Pb*01 yeast cells during the differentiation from mycelium to yeast and on recombinant and native *Pb*ICL enzymes in the presence of different carbon sources. *In silico* analyses were also performed to corroborate the *in vivo* studies (20).

Our results demonstrated that the alkaloid compounds studied inhibited an important enzyme from *Paracoccidioides* spp., namely, the *Pb*MLS. In addition, they inhibited the adhesion of *Pb*18 and *Pb*MLS to the ECM using different cell types and methodologies. Additionally, these alkaloids were not cytotoxic at the concentrations used in the experiments mentioned above. The MICs of compounds 3, 6, and even 8 are remarkably high. On the other hand, compound 4 has moderate activity. Taking both MIC and mammalian toxicity data into consideration, compound 4 is a good candidate for antifungal development. Although in their current form, this class of compounds has modest potency compared with that of amphotericin B or itraconazole, they may offer a basis for the development of alternatives to traditional antifungal agents. Compounds with modest potency have been considered for study (40).

ACKNOWLEDGMENTS

This work, performed at Universidade Federal de Goiás, was supported by the Ministério da Ciência e Tecnologia/Conselho Nacional de Desenvolvimento Científico e Tecnológico (MCTI/CNPq), Fundo Nacional de Desenvolvimento Científico e Tecnológico (FNDCT), Fundação de Amparo à Pesquisa do Estado de Goiás (FAPEG), Coordenação de Aperfeiçoamento de Pessoal de Nível Superior (CAPES), Financiadora de Estudos e Projetos (FINEP), and Instituto Nacional de Ciência e Tecnologia para Inovação Farmacêutica (INCT-IF). Additionally, B.R.D.S.N., R.L.G., and J.D.F.D.S. were supported by fellowships from CNPq, and C.D.S.F. was supported by CAPES.

REFERENCES

1. **Dunn MF, Ramírez-Trujillo JA, Hernández-Lucas I.** 2009. Major roles of isocitrate lyase and malate synthase in bacterial and fungal pathogenesis. Microbiology **155:**3166–3175. http://dx.doi.org/10.1099/mic.0.030858-0.
2. **Zambuzzi-Carvalho PF, Cruz AH, Santos-Silva LK, Goes AM, Soares CMA, Pereira M.** 2009. The malate synthase of *Paracoccidioides brasiliensis* Pb01 is required in the glyoxylate cycle and in the allantoin degradation pathway. Med Mycol **47:**734–744. http://dx.doi.org/10.3109/13693780802609620.
3. **da Silva Neto BR, de Fátima da Silva J, Mendes-Giannini MJ, Lenzi HL, de Almeida Soares CM, Pereira M.** 2009. The malate synthase of *Paracoccidioides brasiliensis* is a linked surface protein that behaves as an anchorless adhesin. BMC Microbiol **9:**272. http://dx.doi.org/10.1186/1471-2180-9-272.
4. **Bastos KP, Bailão AM, Borges CL, Faria FP, Felipe MSS, Silva MG, Martins WS, Fiúza RB, Pereira M, Soares CMA.** 2007. The transcriptome analysis of early morphogenesis in *Paracoccidioides brasiliensis* mycelium reveals novel and induced genes potentially associated to the dimorphic process. BMC Microbiol **7:**29. http://dx.doi.org/10.1186/1471-2180-7-29.
5. **de Arruda Grossklaus D, Bailão AM, Vieira Rezende TC, Borges CL, de Oliveira AM, Parente JA, de Almeida Soares CM.** 2013. Response to oxidative stress in *Paracoccidioides* yeast cells as determined by proteomic analysis. Microb Infect **15:**347–364. http://dx.doi.org/10.1016/j.micinf.2012.12.002.
6. **Ghosh S, Nie A, An J, Huang Z.** 2006. Structure-based virtual screening of chemical libraries for drug discovery. Curr Opin Chem Biol **10:**194–202. http://dx.doi.org/10.1016/j.cbpa.2006.04.002.
7. **Lavecchia A, Di Giovanni C.** 2003. Virtual screening strategies in drug discovery: a critical review. Curr Med Chem **20:**2839–2860. http://dx.doi.org/10.2174/0929867311320999000 1#sthash.96dXApFe.dpuf.
8. **Costa FC, Nicoluci RP, Silva M, Rocha WC, Vieira PC, Oliva G, Thiemann OH, Andricopulo AD.** 2008. Natural products biological screening and ligand-based virtual screening for the discovery of new antileishmanial agents. Lett Drug Des Discov **5:**158–161. http://dx.doi.org/10.2174/157018008784083956.
9. **Bruning JB, Parent AA, Gil G, Zhao M, Nowak J, Pace MC, Smith CL, Afonine PV, Adams PD, Katzenellenbogen JA, Nettles KW.** 2010. Coupling of receptor conformation and ligand orientation determine

graded activity. Nat Chem Biol **6:**837–843. http://dx.doi.org/10.1038/nchembio.451.
10. **Cornejo-Garrido J, Salinas-Sandoval M, Díaz-López A, Jácquez-Ríos P, Arriaga-Alha M, Ordaz-Pichardo C.** 2015. *In vitro* and *in vivo* antifungal activity, liver profile test, and mutagenic activity of five plants used in traditional Mexican medicine. Rev Bras Farmaco **25:**22–28. http://dx.doi.org/10.1016/j.bjp.2014.12.003.
11. **Zhang L, Hua Z, Song Y, Feng C.** 2014. Monoterpenoid indole alkaloids from *Alstonia rupestris* with cytotoxic, antibacterial and antifungal activities. Fitoterapia **97:**142–147. http://dx.doi.org/10.1016/j.fitote.2014.05.018.
12. **Eswar N, John B, Mirkovic N, Fiser A, Ilyin VA, Pieper U, Stuart AC, Marti-Renom MA, Madhusudhan MS, Yerkovich B, Sali A.** 2003. Tools for comparative protein structure modeling and analysis. Nucleic Acids Res **31:**3375–3380. http://dx.doi.org/10.1093/nar/gkg543.
13. **Zhang Y.** 2008. I-TASSER server for protein 3D structure prediction. BMC Bioinformatics **9:**40. http://dx.doi.org/10.1186/1471-2105-9-40.
14. **Colovos C, Yeates TO.** 1993. Verification of protein structures: patterns of nonbonded atomic interactions. Protein Sci **9:**1511–1519.
15. **Lovell SC, Davis IW, Arendall WB, III, de Bakker PIW, Word JM, Prisant JMMG, Richardson DC.** 2003. Structure validation by Cα geometry: ϕ,ψ and Cβ deviation. Proteins **50:**437–450. http://dx.doi.org/10.1002/prot.10286.
16. **Lüthy R, Bowie JU, Eisenberg D.** 1992. Assessment of protein models with three-dimensional profiles. Nature **356:**83–85. http://dx.doi.org/10.1038/356083a0.
17. **Berendsen HJC, van der Spoel D, van Drunen R.** 1995. Gromacs: a message-passing parallel molecular dynamics implementation. Comput Phys Commun **91:**43–56. http://dx.doi.org/10.1016/0010-4655(95)00042-E.
18. **Lindahl E, Hess B, van der Spoel D.** 2001. GROMACS 3.0: a package for molecular simulation and trajectory analysis. J Mol Model **7:**306–317.
19. **Pronk S, Páll S, Schulz R, Larsson P, Bjelkmar P, Apostolov R, Shirts MR, Smith JC, Kasson PM, van der Spoel D, Hess B, Lindahl E.** 2013. GROMACS 4.5: a high-throughput and highly parallel open source molecular simulation toolkit. Bioinformatics **29:**845–854. http://dx.doi.org/10.1093/bioinformatics/btt055.
20. **do Prado RS, Alves RJ, de Oliveira CMA, Kato L, da Silva RA, Quintino GO, do Desterro Cunha S, de Almeida Soares CM, Pereira M.** 2014. Inhibition of *Paracoccidioides lutzii Pb*01 isocitrate lyase by the natural compound argentilactone and its semi-synthetic derivatives. PLoS One **9:**e94832. http://dx.doi.org/10.1371/journal.pone.0094832.
21. **Irwin JJ, Shoichet BK.** 2005. ZINC–a free database of commercially available compounds for virtual screening. J Chem Inf Model **45:**177–182. http://dx.doi.org/10.1021/ci049714+.
22. **Schüttelkopf AW, van Aalten DMF.** 2004. PRODRG: a tool for high-throughput crystallography of protein-ligand complexes. Acta Crystallogr D Biol Crystallogr **60:**1355–1363. http://dx.doi.org/10.1107/S0907444904011679.
23. **Trott O, Olson AJ.** 2010. AutoDock Vina: improving the speed and accuracy of docking with a new scoring function, efficient optimization, and multithreading. J Comput Chem **31:**455–461. http://dx.doi.org/10.1002/jcc.21334.
24. **Volkamer A, Griewel A, Grombacher T, Rarey M.** 2010. Analyzing the topology of active sites: on the prediction of pockets and subpockets. J Chem Inf Model **50:**2041–2052. http://dx.doi.org/10.1021/ci100241y.
25. **Abad-Zapatero C.** 2007. Ligand efficiency indices for effective drug discovery. Expert Opin Drug Discov **2:**469–488. http://dx.doi.org/10.1517/17460441.2.4.469.
26. **Kato L, de Oliveira CMA, Faria EO, Ribeiro LC, Carvalho BG, da Silva CC, Schuquel ITA, Santin SMO, Nakamura CV, Brita E, Miranda N, Iglesias AH, Delprete PG.** 2012. Antiprotozoal alkaloids from *Psychotria prunifolia* (Kunth) Steyerm. J Braz Chem Soc **23:**355–360. http://dx.doi.org/10.1590/S0103-50532012000200024.
27. **de Freitas CS, Silva D, Kato LL, de Oliveira CMA, Schuquel IT, da Silva CC, Santin SDO, Delprete PG, Neto BRDS, Soares CMA, Pereira M.** 2012. New β-carboline alkaloids from *Galianthe ramosa* (*Rubiaceae*). Planta Med **78:**169. http://dx.doi.org/10.1055/s-0032-1320857.
28. **Kato L, Marques Braga R, Sumiko Kinoshita L.** 2002. Indole alkaloids from *Rauvolfia bahiensis* A.DC. (*Apocynaceae*). Phytochemistry **60:**315–320. http://dx.doi.org/10.1016/S0031-9422(02)00122-X.
29. **Roucourt B, Minnebo N, Augustijns P, Hertveldt K, Volckaert G, Lavigne R.** 2009. Biochemical characterization of malate synthase G of *P. aeruginosa*. BMC Biochem **10:**20. http://dx.doi.org/10.1186/1471-2091-10-20.
30. **Ornston LN, Ornston MK.** 1969. Regulation of glyoxylate metabolism in *Escherichia coli* K-12. J Bacteriol **98:**1098–1108.
31. **Beeckmans S, Khan AS, Kanarek L, Van Driessche E.** 1994. Ligand binding on to maize (*Zea mays*) malate synthase: a structural study. Biochem J **303:**413–421.
32. **Fava-Netto C.** 1955. Quantitative studies on fixation of complement in South American blastomycosis with polysaccharide antigen. Arq Cir Clín Exp **18:**197–254.
33. **Clinical and Laboratory Standards Institute.** 2008. Reference method for broth dilution antifungal susceptibility testing of yeasts; approved standard–3rd ed. CLSI document M27-A3. Clinical and Laboratory Standards Institute, Wayne, PA.
34. **de Paula e Silva AC, Oliveira HC, Silva JF, Sangalli-Leite F, Scorzoni L, Fusco-Almeida AM, Mendes-Giannini MJ.** 2013. Microplate alamarBlue assay for *Paracoccidioides* susceptibility testing. J Clin Microbiol **51:**1250–1252. http://dx.doi.org/10.1128/JCM.02914-12.
35. **Malvern.** 1998. ITC data analysis in origin tutorial guide, version 5. Malvern, Worcestershire, United Kingdom. http://www.bioch.ox.ac.uk/aspsite/services/equipmentbooking/biophysics/ITC_data_analysis.pdf.
36. **Mendes-Giannini MJ, Hanna SA, da Silva JL, Andreotti PF, Vincenzi LR, Benard G, Lenzi HL, Soares CP.** 2004. Invasion of epithelial mammalian cells by *Paracoccidioides brasiliensis* leads to cytoskeletal rearrangement and apoptosis of the host cell. Microb Infect **6:**882–891. http://dx.doi.org/10.1016/j.micinf.2004.05.005.
37. **Mosmann T.** 1983. Rapid colorimetric assay for cellular growth and survival: application to proliferation and cytotoxicity assays. J Immunol Methods **65:**55–63. http://dx.doi.org/10.1016/0022-1759(83)90303-4.
38. **Zambuzzi-Carvalho PF, Tomazett PK, Santos SC, Ferri PH, Borges CL, Martins WS, Soares CMDA, Pereira M.** 2013. Transcriptional profile of *Paracoccidioides* induced by oenothein B, a potential antifungal agent from the Brazilian Cerrado plant *Eugenia uniflora*. BMC Microbiol **13:**227. http://dx.doi.org/10.1186/1471-2180-13-227.
39. **Santos GD, Ferri PH, Santos SC, Bao SN, Soares CMA, Pereira M.** 2007. Oenothein B inhibits the expression of *Pb*FKS1 transcript and induces morphological changes in *Paracoccidioides brasiliensis*. Med Mycol **45:**609–618. http://dx.doi.org/10.1080/13693780701502108.
40. **Burrows LL, Stark M, Chan C, Glukhov E, Sinnadurai S, Deber CM.** 2006. Activity of novel non-amphipathic cationic antimicrobial peptides against *Candida* species. J Antimicrob Chemother **57:**899–907. http://dx.doi.org/10.1093/jac/dkl056.